LANGMUIR

pubs.acs.org/Langmuir Article

Electrochemical Quantification of Corrosion Mitigation on Iron Surfaces with Gallium(III) and Zinc(II) Metallosurfactants

A. D. K. Isuri Weeraratne, Chathuranga C. Hewa-Rahinduwage, Long Luo,* and Cláudio N. Verani*

Cite This: *Langmuir* 2020, 36, 14173−14180 Read Online

ACCESS | Metrics & More | Article Recommendations | Supporting Information

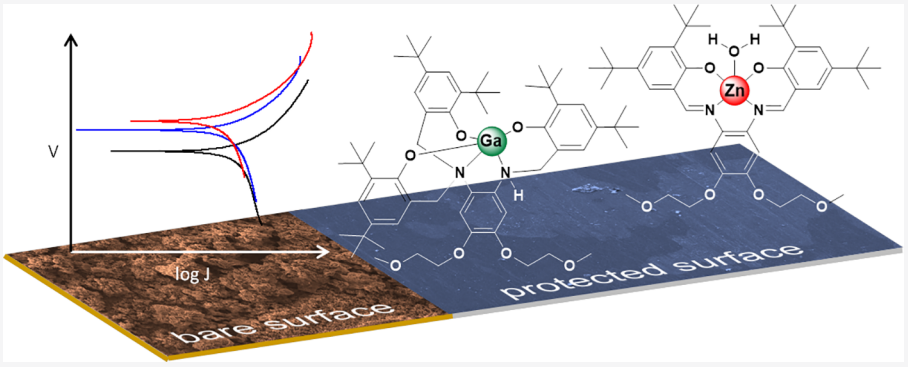

ABSTRACT: We have recently described a new potential use for Langmuir−Blodgett films of surfactants containing redox-inert metal ions in the inhibition of corrosion and have shown good qualitative results for both iron and aluminum surfaces. In this study we proceed to quantify electrochemically the viability of gallium(III)- and zinc(II)-containing metallosurfactants $[Ga^{III}(L^{N2O3})]$ (**1**) and $[Zn^{II}(L^{N2O2})H_2O]$ (**2**) as mitigators for iron corrosion in saline and acidic media. We evaluate their charge transfer suppression and then focus on potentiodynamic polarization and impedance spectroscopy studies, including detailed SEM data to interrogate their metal dissolution/oxygen reduction rate mitigation abilities. Both complexes show some degree of mitigation, with a more pronounced activity in saline than in acidic medium.

INTRODUCTION

Corrosion is the deterioration of a metal surface caused by chemical and electrochemical interaction with its surrounding environment. It is an inevitable problem confronted by almost all industries at an annual cost of $2.5 trillion, equivalent to 3.4% of the global gross domestic product.[1] Aqueous iron corrosion consists of an anodic reaction which causes metal dissolution as Fe^{2+} ions and the cathodic reduction of H^+ and O_2 present in the electrolyte solution. Saline and acidic media expedite iron corrosion because they facilitate and intensify electron transfer,[2] leading to the formation of hydrated iron(III) oxide or $Fe_2O_3{\cdot}xH_2O$, the thermodynamically stable product known as rust.[3,4]

The search for corrosion prevention strategies may lead to considerable global savings,[1,5] and the use of protective coatings can be beneficial to the preservation of iron surfaces.[6,7] Coatings usually consist of layered protective systems encompassing pretreatment, primer, and top coat. Relevant to this study, the pretreatment layer is directly physisorbed or chemisorbed to the metal surface and chromium(III)-based systems have been traditionally favored.[8,9] Environmental concerns with hexavalent chromium impose steep restrictions to the use of chromium-based coatings.[10] The discovery of new and more benign inhibitors has attracted considerable attention,[11−19] and surfactants figure among well-known molecular inhibitors.[3,20−29]

We recently reported on Langmuir−Blodgett (LB) films of phenolate-rich metallosurfactants $[Ga^{III}(L^{N2O3})]$ (**1**) and $[Zn^{II}(L^{N2O2})H_2O]$ (**2**) that seem to behave as a surface pretreatment for corrosion inhibition on iron[30] and aluminum[31] surfaces. Metallosurfactants **1** and **2** are designed to contain hydrophobic *tert*-butyl groups installed to the phenolates along with hydrophilic alkoxy chains installed to a phenylenediamine bridge that enable physisorption to the metal surface. These species accommodate the redox-inert $3d^{10}$ ions gallium(III) and zinc(II) (Figure 1) in order to confer added structural resistance to the organic framework and increase the energies of empty ligand-based molecular orbitals (LUMOs), precluding electron transfer through the film. As a consequence, these species show qualitative mitigation of the

Received: June 19, 2020
Revised: November 9, 2020
Published: November 18, 2020

https://dx.doi.org/10.1021/acs.langmuir.0c01826
Langmuir 2020, 36, 14173−14180

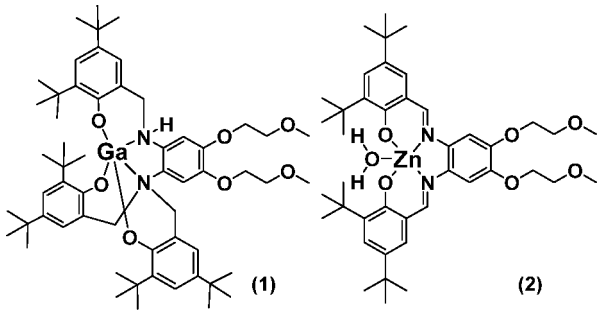

Figure 1. Metallosurfactants $[Ga^{III}(L^{N2O3})]$ (**1**) and $[Zn^{II}(L^{N2O2})H_2O]$ (**2**).

corrosive process.[30,31] Those studies were focused on nonelectrochemical techniques based on weight loss[32] and SEM measurements to assess corrosion inhibition on iron surfaces. Because a quantitative analysis of the mitigation abilities of these materials to prevent metal dissolution and oxygen reduction is still lacking, in this study we assess the properties of **1** by nonelectrochemical methods and compare with those of **2** and then use the more sophisticated electroanalytical techniques of impedance spectroscopy and potentiodynamic polarization. This comprehensive evaluation enables a more complete characterization of the corrosion mitigation behavior of these species and informs about the viability and limitations of these metallosurfactants in mitigating corrosion.

RESULTS AND DISCUSSION

Synthesis of the Metallosurfactants. The species $[Ga^{III}(L^{N2O3})]$ (**1**) and $[Zn^{II}(L^{N2O2})H_2O]$ (**2**) were synthesized as reported by us elsewhere.[30,31] In brief, the ligand H_3L^{N2O3} was obtained by treating 4,5-bis(2-methoxyethoxy)-benzene-1,2-diamine with 2,4-di-*tert*-butyl-6-(chloromethyl)-phenol in the presence of triethylamine, while H_2L^{N2O2} was synthesized by treating the above mentioned diamine precursor with 3,5-di-*tert*-butyl-2-hydroxybenzaldehyde under an inert atmosphere in methanol under reflux.[33,34] Species **1** was obtained by treatment of 1 equiv of the purified H_3L^{N2O3} ligand with 1 equiv of $GaCl_3$,[31] whereas **2** was synthesised by treating 1 equiv of H_2L^{N2O2} with 1 equiv of $Zn^{II}Cl_2{\cdot}6H_2O$ under refluxing conditions.[30] Both procedures require the presence of $NaOCH_3$ to deprotonate the phenol groups into coordinating phenolates.

Interfacial Properties. The interfacial properties that lead to the formation of mono- and multilayered LB films by $[Ga^{III}(L^{N2O3})]$ (**1**) and $[Zn^{II}(L^{N2O2})H_2O]$ (**2**) were studied using surface pressure (π, mN/m) vs average molecular area (A, Å^2/molecule) isothermal compression and Brewster angle microscopy (BAM) at 23 ± 1 °C.[30,31] The isothermal compression curve for **1** (Figure S1a) at the air/water interface showed an area of intermolecular interaction at approximately 120 Å^2/molecule. An initially homogeneous Langmuir−Pockels[35] (LP) film with no remarkable BAM activity was observed between 10 and 27. Compression of this liquid-expanded film was followed by phase rearrangement between 28 and 37 mN/m to yield another homogeneously looking condensed phase film between 38 and 45 mN/m. BAM data (Figure S1b) reveals the formation of granular texture above 42 mN/m as the compressed monolayer becomes thermodynamically unstable and forms localized multilayer regions that lead to film collapse at approximately 47−48 mN/m following a constant pressure mechanism.[36−39] Interaction for **2** starts at around 60 Å^2/molecule with further compression of the LB film yielding a homogeneous film between 10 and 44 mN/m (Figure S1c). Although a minor change in slope is visible at ∼30 mN/m, uneventful BAM images support the formation of a homogenous film. Like for the more obvious **1** this change is likely associated with a phase transition. An area of about 65 Å^2/molecule is registered at 45 mN/m, prior to collapse. BAM images reveal the presence of arrays of Newton rings (Figure S1d). Langmuir−Blodgett (LB) films were deposited on glass substrates as Y-type multilayers while keeping the transfer ratio close to unity and were studied using infrared reflection absorption spectroscopy (IRRAS) with p-polarized light at 40° and 20° incidence for **1** and **2**.[30,31] The films for both species displayed asymmetric and symmetric C−H stretching vibrations between 2860 and 2960 cm^{-1}, therefore slightly shifted from the asymmetric C−H stretching vibrations observed in bulk. Other bands observed around 1350−1610 cm^{-1} are associated with aromatic C=C stretching vibrations and CH_n deformation bands. Species **2** shows a band at 1592 cm^{-1} assigned to the C=N stretching of the imine ligand. Allied to previous IRRAS and static contact measurement studies,[30,40] these results confirm that the hydrophilic ethoxymethoxy chains of species **1** and **2** interact with the iron substrate by physisorption while the *tert*-butyl-decorated phenolates that envelop the metal centers groups point outwards. While a stronger covalent interaction would be beneficial, this molecular arrangement enhances the hydrophobicity of the surface to be protected.

Charge Transfer Suppression by Metallosurfactants. Cyclic voltammetry experiments were performed to determine whether LB films of **1** and **2** suppress electron transport on gold electrodes. An aqueous 1.0 × 10^{-3} M $K_3[Fe^{III}(CN)_6]$ solution in 0.1 M KCl was added to a standard three-electrode cell equipped with gold plates coated with 1−13 LB layers of **1** and **2** at room temperature. The coated gold plates were used as working electrodes, whereas Ag/AgCl and Pt wire were respectively used as the reference and auxiliary electrodes. Initially, the reversible redox wave associated with the $[Fe^{III}(CN)_6]^{3-}/[Fe^{II}(CN)_6]^{4-}$ couple was observed for bare gold electrodes but decreased significantly upon coating with a monolayer of **1** or **2**. To optimize the most adequate deposition pressures that yield ordered films able to suppress charge transfer, monolayers were deposited on gold substrates at three different surface pressures, namely, 20, 30, and 40 mN/m. These surface pressures are associated with respective average molecular areas of 80, 64, and 35 Å^2/molecule for **1** and 51, 47, and 44 Å^2/molecule for **2** and are related to film uniformity. Best suppression was observed in monolayers deposited at 40 mN/m for **1**, while 30 mN/m worked best for **2**. As the number of insulating LB layers increased, charge transfer between the $[Fe^{III/II}(CN)_6]^{3-}$ species and the electrode became less and less pronounced, being negligible after 10 layers. Near complete charge suppression was attained at 13 layers for **1**, with a residual current of 0.006 mA, and at 11 layers for **2** with a current of 0.002 mA.[30,31] The stability of the deposited LB films was tested under acidic conditions by immersing each of the gold electrodes protected by either 13 layers of **1** or 11 layers of **2** in 0.01 M H_2SO_4 for 3, 5, and 8 days. Figure 2 shows charge transfer suppresion of gold electrodes with **1**. The stability of ligands H_3L^{N2O3} and H_2L^{N2O2} was also studied in acidic solution (Figure S2). Impressively, the maximum current for both metallosurfactants only reached a maximum of 0.02 mA, while the ligands showed

https://dx.doi.org/10.1021/acs.langmuir.0c01826
Langmuir 2020, 36, 14173−14180

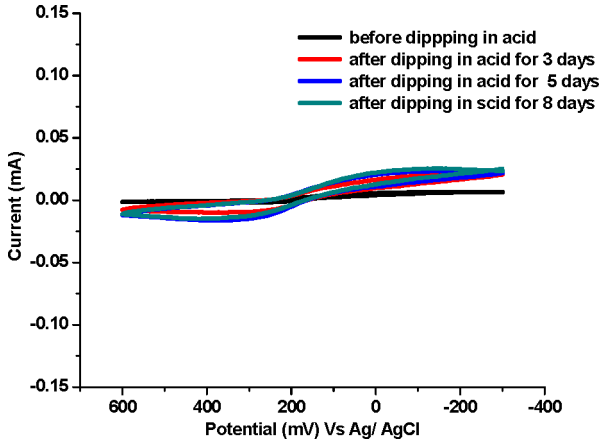

Figure 2. CVs for charge transfer suppression with 13 LB monolayers of **1**, before and after dipping in acidic media. Scan rates: 100 mV s^{-1} in all experiments.

higher currents of 0.05 and 0.06 mA, respectively.[30] This result confirms that the metallosurfactants withstand the acidic environment and retain their metal centers.

Qualitative Corrosion Analysis. Iron corrosion is an electrochemical process that depends on the concentration of oxygen, iron(II) and iron(III) species, pH, and presence of electrolytes to trigger complex mechanisms. Under aerobic conditions, the main steps can be summarized by the semireactions listed in eqs 1−4:

$$2Fe^{0}_{(s)} \rightarrow 2Fe^{2+}_{(aq)} + 4e^{-} \quad \text{(anodic)} \tag{1}$$

$$O_{2(g)} + 2H_2O_{(l)} + 4e^{-} \rightarrow 4OH^{-}_{(aq)} \quad \text{(cathodic)} \tag{2}$$

$$Fe^{2+} + 2OH^{-}_{(aq)} \rightarrow Fe(OH)_{2(s)} \tag{3}$$

$$Fe(OH)_{2(s)} + O_{2(g)} \rightarrow Fe_2O_3{\cdot}xH_2O_{(s)} \tag{4}$$

The cathodic step is determinant, and rates of reaction for each of the above steps increase significantly when in acidic or saline media, where electron transfer is facilitated.[2] Materials able to mitigate corrosion must withstand such conditions and prevent either the anodic dissolution of the metal (eq 1) or the cathodic reduction of oxygen (eq 2). The effect of these media on 99.5% iron surfaces coated by LB films of $[Ga^{III}(L^{N2O3})]$ (**1**) can be investigated by ferroxyl staining and compared to that of $[Zn^{II}(L^{N2O2})H_2O]$ (**2**).[30] Iron substrates measuring 10 mm × 25 mm are placed in a Petri dish filled with warm agar containing the acid−base indicator phenolphthalein, potassium ferricyanide $K_3[Fe^{III}(CN)_6]$, and either 3% NaCl or 0.01 M H_2SO_4. Upon cooling, the agar forms a semisolid gel that encases the substrate while the indicators are used to identify the corrosion processes taking place in the anode and in the cathode. Phenolphthalein, colorless in acidic and neutral media, turns pink in the presence of OH^- ions at the cathode, indicating the absence of iron oxidation. Potassium ferricyanide reacts with Fe^{2+} ions formed during the corrosion process yielding a visible Prussian blue complex at the anode. Experiments were performed with iron substrates having half of their length covered with 13 layers of **1**, whereas the other half is left bare; the substrates are exposed to both saline and acidic media over a course of 1 and 7 days. For emphasis on the iron degradation process, experiments were also carried out in the absence of phenolphthalein (Figure 3 and Figure S3). In

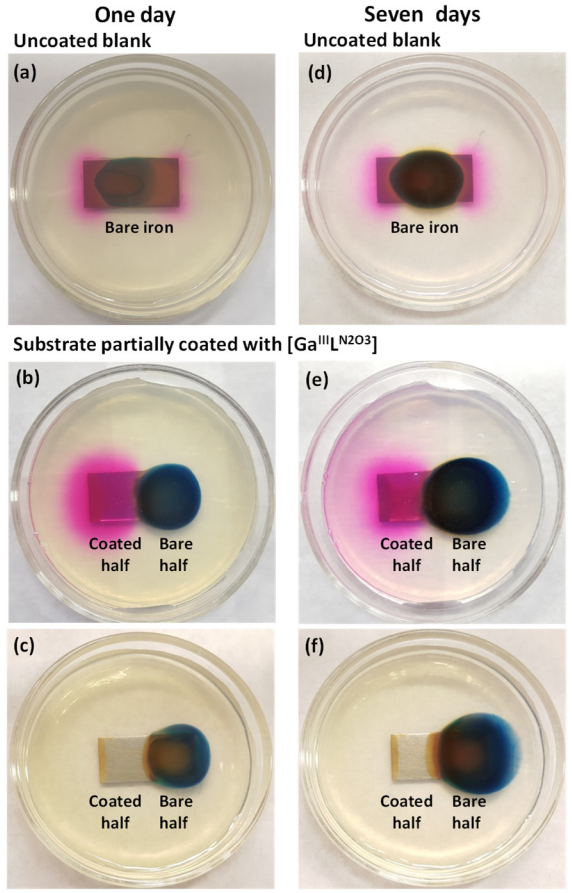

Figure 3. Ferroxyl staining for saline corrosion after 1 and 7 days: bare substrates in (a) and (d), substrates coated with 13 layers of **1** in (b) and (e), and substrates coated with 13 layers of **1** without phenolphthalein in (c) and (f).

both experiments, no blue coloration associated with Fe^{2+} generation was observed in the coated region, indicating that the film acts as a corrosion protection barrier in both acidic and saline media. This protective behavior indicates that iron oxidation and dissolution are substantially curbed, although oxygen reduction persists. Because iron(II) generation is mitigated, formation of rust, as described in eqs 3 and 4, is partialy prevented. A similar response is observed for metallosurfactant **2**.[30]

Scanning electron micrograph (SEM) images were recorded to evaluate the formation and agglomeration of $Fe_2O_3{\cdot}xH_2O_{(s)}$, rust, on the iron substrates immersed in 0.01 M H_2SO_4 and 0.1 M NaCl solutions for 5 days. In acidic medium, the bare section of the iron substrates exhibited well-defined granular rust formation, while corrosion was inhibited in the section coated with LB films of **1**. In saline medium, iron plates were degrading with the formation of an insoluble black material visually similar to magnetite-like Fe_3O_4. In saline medium, the bare section of the iron substrates showed a rougher surface compared to the coated section (Figure 4). Metallosurfactant **2** showed visually similar results reported elsewhere.[30]

Quantitative Corrosion Analysis. We carried out potentiodynamic polarization and electrochemical impedance spectroscopy measurements to quantify the ability of metallosurfactants $[Ga^{III}(L^{N2O3})]$ (**1**) and $[Zn^{II}(L^{N2O2})H_2O]$ (**2**) to act on metal dissolution (eq 1) or on oxygen reduction (eq 2). Potentiodynamic polarization experiments provide information

https://dx.doi.org/10.1021/acs.langmuir.0c01826
Langmuir 2020, 36, 14173−14180

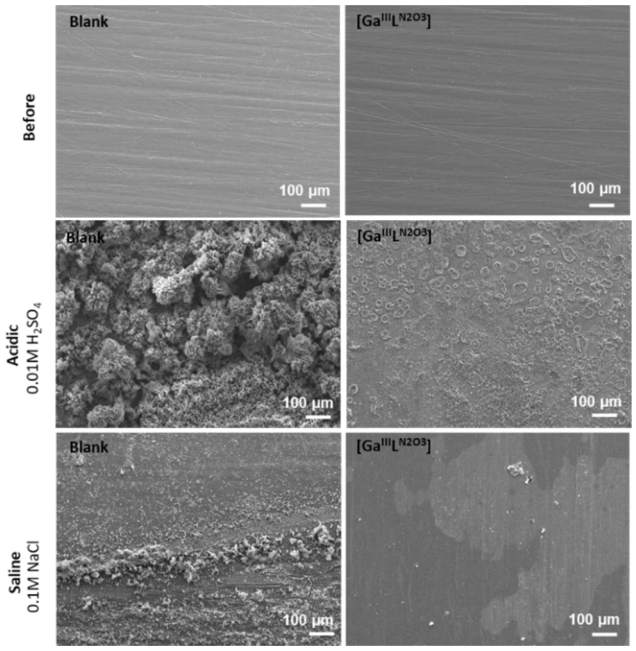

Figure 4. SEM images for the unprotected blank and for the 13-layer LB film-deposited iron substrates: before and after acidic and saline corrosion.

on the corrosion potential and current density and were performed using a three-electrode setup, where iron substrates were used as the working electrode, a Pt wire as the auxiliary electrode, and Ag/AgCl as the reference electrode. We evaluated the corrosion inhibition ability of **1** and **2** in saline and acidic solution by immersing the metallosurfactant-coated iron substrates in a 3.5% NaCl or 0.01M H_2SO_4 for 30 min before the electrochemical measurement. Corrosion currents (i_{corr}) and corrosion potentials (E_{corr}) were obtained by extrapolating the small linear parts of both anodic and cathodic polarization curves known as Tafel lines to their intersection (see Figure S4).[41] If the displacement leads to $E > E_{corr}$, anodic polarization for metal oxidation in E_{corr} informs the inhibition activity. If it is greater than 85 mV/E_{corr}, either the cathodic or anodic steps are inhibited. For displacements smaller than 85 mV/E_{corr} a mixed type mitigation takes place and both anodic and cathodic steps are affected. The Tafel slopes β_a and β_c inform about the anodic and cathodic polarization constants and the possible alterations of mechanisms by which corrosion takes place. Inhibition efficiencies (IE_{pol}%) were calculated using eq 5.[42]

$$IE_{pol}\% = (i_{corr} - i'_{corr}/i_{corr}) \times 100 \quad (5)$$

where i_{corr} and i'_{corr} are the corrosion current values of the bare and coated substrates, respectively. Table 1 summarizes the data.

In saline medium there is a significant decrease in the corrosion currents for the LB-coated substrates, as compared to the bare iron substrates. The corrosion current for the bare iron reached 64 ± 4 μA/cm^2, whereas the iron substrate protected with either the Ga-containing **1** or the Zn-containing **2** showed respective corrosion currents of 40 ± 9 μA/cm^2 and 32 ± 7 μA/cm^2 with averaged IE_{pol}% of 38% for **1** and 50% for **2**. This decrease indicates that these metallosurfactants mitigate the corrosion process. The E_{corr} shifts towards less negative potentials, thus indicating that the modified surfaces

Table 1. Electroanalytic Parameters

sample		E_{corr} (mV)	i_{corr} (μA/cm^2)	β_a (mV/dec)	β_c (mV/dec)	avg IE_{pol} (%)
saline	blank	−542	64 ± 4	128.1	−525.9	
	1	−468	40 ± 9	119.3	−426.8	38
	2	−438	32 ± 7	101.8	−437.7	50
acidic	blank	−561	167 ± 9	92.9	−193.1	
	1	−559	145 ± 3	86.8	−176.0	13
	2	−556	137 ± 5	88.7	−177.0	18

are more resistant to corrosion than the bare substrates. With the metallosurfactants, the anodic curves move toward a lower current density region, while the variations of cathodic curves are not obvious. This phenomenon suggests that mitigation takes place by limiting the anodic reaction of metal dissolution (eq 1). This is in good agreement with the ferroxyl staining shown in Figure 3. The variability of the cathodic and anodic slopes (β_c and β_a) with the presence of molecular films implies that oxygen reduction and metal dissolution were affected without modifying the mechanism of corrosion.[43] Substrates with deposited films also showed more positive corrosion potentials of −468 $mV_{Ag/AgCl}$ and −438 $mV_{Ag/AgCl}$ for **1** and **2** than for bare iron substrates (−542 $mV_{Ag/AgCl}$), further confirming the inhibition efficiency of both metallosurfactants.[44]

Similar results were found for corrosion tests in acid. The i_{corr} and E_{corr} of the bare iron substrates reached 167 ± 9 μA/cm^2 and −561 $mV_{Ag/AgCl}$, respectively. Substrates coated with metallosurfactant **1** showed a corrosion current and corrosion potential of 145 ± 3 μA/cm^2 and −559 $mV_{Ag/AgCl}$, while these two values for substrates coated with **2** are 137 ± 5 μA/cm^2 and −556 $mV_{Ag/AgCl}$, respectively. Similar to the results for saline, E_{corr} shifts toward less negative values associated with metal dissolution mitigation, although with a considerably lower variation. On the basis of these results, the average IE_{pol}% value for **1** was calculated at 13%, whereas that of **2** was found at 18%. These observations suggest that coated substrates show higher inhibition efficiency in the saline medium compared to the acidic medium (Figure 5 and Figure S5).

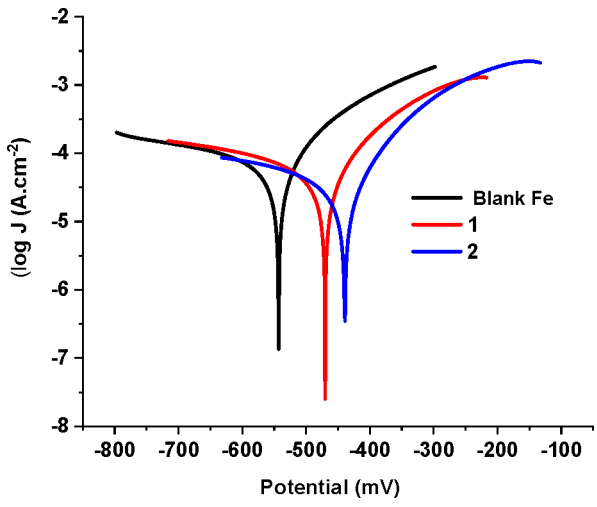

Figure 5. Potentiodynamic polarization curves for **1** and **2** after 30 min exposure to 3.5% NaCl. Scan rate: 10 mV s^{-1}.

https://dx.doi.org/10.1021/acs.langmuir.0c01826
Langmuir 2020, 36, 14173−14180

Electrochemical impedance spectroscopy was used to further assess the corrosion inhibition ability of the films of metallosurfactants **1** and **2**. Figure 6 shows the Nyquist plots

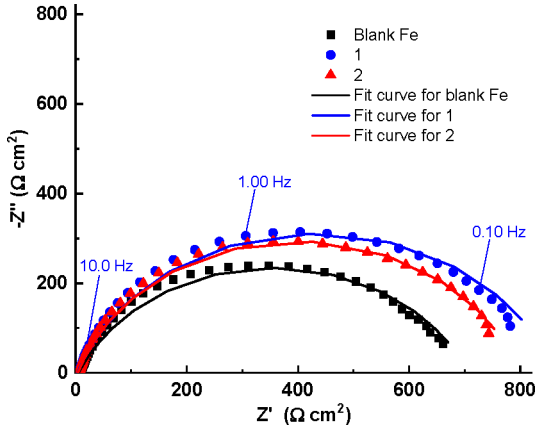

Figure 6. Nyquist plots for iron substrates and blank and coated with LB films of **1** and **2** immersed in 3.5% NaCl.

of the bare iron substrates and iron substrates coated with the metallosurfactants **1** and **2** in 3.5% NaCl. Charge transfer resistance (R_{ct}) values were obtained by fitting the data to an equivalent circuit (Figure S6, Table S1). Inhibition efficiencies (IE_{imp}%) from charge transfer resistance (R_{ct}) was calculated using eq 6.[26,43,45]

$$IE_{imp}\% = \frac{R'_{ct} - R_{ct}}{R'_{ct}} \times 100 \quad (6)$$

where R'_{ct} and R_{ct} are the charge transfer resistance of the LB-film coated substrate and the bare substrate, respectively. In 3.5% NaCl, iron substrates coated with **1** and **2** showed a notably higher R_{ct} than the observed for the bare substrate (825.7 and 802.8 Ω·cm^2 vs 703.0 Ω·cm^2, respectively). Substrates coated with **1** and **2** showed respective inhibition efficiencies of 15% and 12%. Similar measurements were performed in 0.01 M H_2SO_4. All iron substrates showed significantly smaller R_{ct} values in H_2SO_4 than those in 3.5% NaCl (Figure S7, Table S2). Nonetheless, the substrates coated with **1** and **2** still showed slightly higher R_{ct} values than bare iron, indicating some degree of corrosion inhibition.

Acidic Mitigation and Coordination Chemistry. All methods used in this study point to two observations: (i) the metallosurfactants $[Ga^{III}(L^{N2O3})]$(**1**) and $[Zn^{II}(L^{N2O2})H_2O]$ (**2**) act predominantly on the anodic reaction associated with metal dissolution (eq 1), and (ii) the mitigation activity is pronounced in saline and modest in acidic media. In fact the anodic process described in eq 1 is best described as

$$Fe^0_{(s)} + 6H_2O \rightarrow [Fe^{II}(H_2O)_6]^{2+} + 2e^- \quad (7)$$

Because the rates of corrosion depend heavily on the presence of acids and electrolytes, sulfuric acid self-regenerates in the presence of Fe^{2+} perpetuating the corrosion process that can be summarized in eqs 5−8 as follows:[46]

$$Fe^{2+}_{(aq)} + SO_4^{2-}{}_{(aq)} \rightarrow FeSO_{4(aq)} \quad (8)$$

$$2Fe^{3+}_{(aq)} + 3SO_4^{2-}{}_{(aq)} \rightarrow Fe_2(SO_4)_{3(aq)} \quad (9)$$

$$4FeSO_4 + O_2 + 6H_2O \rightarrow 2Fe_2O_3{\cdot}xH_2O_{(s)} + 4H_2SO_{4(aq)} \quad (10)$$

$$4H_2SO_{4(aq)} + 4Fe^{2+}_{(aq)} + 2O_2 \rightarrow 4FeSO_{4(aq)} + 4H_2O \quad (11)$$

Therefore, in aqueous solution the salts descibed as $FeSO_4$ and $Fe_2(SO_4)_3$ are the complex octahedral species hexaaqua-ferrous and hexaaquaferric sulfates $[Fe^{II}(H_2O)_6](SO_4)$ and $[Fe^{III}(H_2O)_6]_2(SO_4)_3$, respectively. This self-regenerating acidic environment may enable localized high-concentrations of iron sufficient to compete with the Ga^{3+} and Zn^{2+} ions coordinated to the ligands that form metallosurfactants **1** and **2**. To test this possibility, we have treated wet methanolic solutions of 1.0×10^{-4} M **1** and 1.0×10^{-5} M **2** with 0.25, 0.5, and 1 equiv of $FeCl_2$ and $FeCl_3{\cdot}6H_2O$ salts and followed the spectroscopic changes that take place (Figure 7, Figure S8).

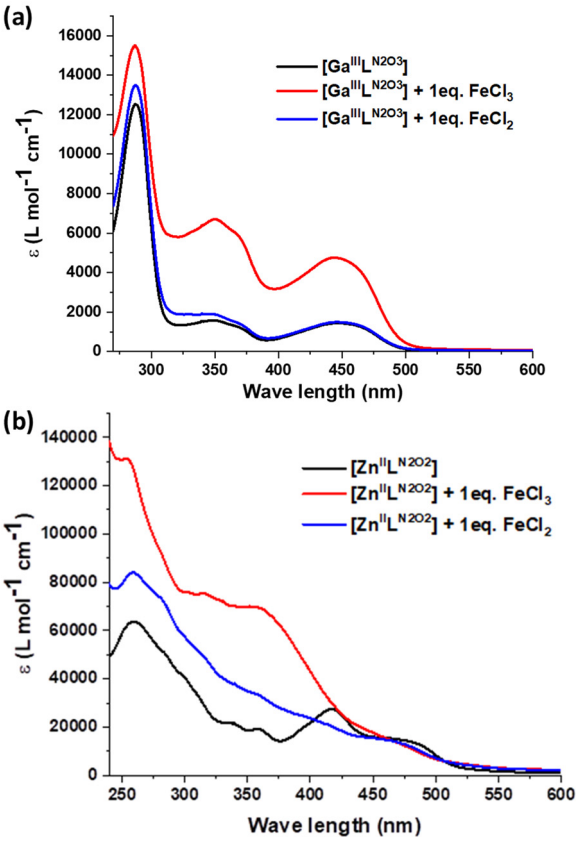

Figure 7. Spectral changes related to the addition of 1 equiv of $FeCl_2{\cdot}xH_2O$ and $FeCl_3{\cdot}xH_2O$ to (a) **1** and (b) **2** in methanol.

$[Ga^{III}(L^{N2O3})]$ (**1**) has bands at 287 (ε = 12 460), 348 (1580), 448 nm (1470 M^{-1} cm^{-1}), and the addition of Fe^{II} led to negligible changes. However, the aerobic environment and the triply negative pocket in the ligand $(L^{N2O3})^{3-}$ strongly favor Fe^{III} coordination. In this case prominent changes were observed when 1 equiv of Fe^{III} was added to **1**; the band at 287 nm increased its ε to 16 000 and was followed by a broad and complex area with three overlapping bands at approximately 330, 350, and 370 nm of similar $\varepsilon \approx 5000$, while the band at 448 nm doubled its intensity to 2900 M^{-1} cm^{-1} and displayed a shoulder at ∼460 nm. This behavior indicates the presence of multiple species. However, the more intense band at 287 nm and those at 330 and 370 nm are relevant because

https://dx.doi.org/10.1021/acs.langmuir.0c01826
Langmuir 2020, 36, 14173−14180

they coincide with the previously reported[34] spectrum for the isolated and characterized $[Fe^{III}(L^{N2O3})]$. The last two bands are diagnostic of phenolate-to-Fe^{III} charge transfer and can be detected in solutions containing $[Ga^{III}(L^{N2O3})]$:Fe^{III} ratios of 2:1 and 4:1, confirming that replacement of Ga by Fe ions in **1** is a relevant mechanism of deactivation and explaining the marginal mitigation provided by this species when in acidic media.

The behavior of the zinc-containing $[Zn^{II}(L^{N2O2})H_2O]$ (**2**) is more subtle due to the large number of bands that arise from a square-planar environment. This species has bands at 251 (ε = 26 400), 304 (21 700), 337 (15 350), 358 (15 100), 417 (25 000), and 472 nm (12 300 M^{-1} cm^{-1}), while its previously published[33] analogue $[Fe^{II}(L^{N2O2})Cl]$ shows bands at 310 (49 900), 351 (40 360), 395 (30 520), and 447 nm (19 210 M^{-1} cm^{-1}). Addition of both Fe^{II} and Fe^{III} maintains the original band positions while changing their ε values. The most dramatic change is the decrease of the band at 417 mn in the presence of Fe^{II} and the increase of the bands between 300 and 400 nm in the presence of Fe^{III} ions. These changes also convey that metal replacement can take place when a critical concentration of iron is attained.

CONCLUSIONS

Both metallosurfactants $[Ga^{III}(L^{N2O3})]$ (**1**) and $[Zn^{II}(L^{N2O2})H_2O]$ (**2**) show the ability to preclude electron transfer from the environment to the iron surface and prevent to some extent the anodic reaction associated with metal dissolution. These species do not seem to influence the cathodic reaction associated with oxygen reduction or alter the mechanisms of corrosion. The extent of the mitigation activity depends on the metallosurfactant and on the media used. Although **1** is a more efficient mitigator than **2**, both species show better activity in saline medium. Their inhibition in acidic medium is much less pronounced, possibly because self-regeneration of H_2SO_4 builds up trivalent Fe ions in concentrations sufficient to compete with gallium(III) in **1** and zinc(II) in **2**.

EXPERIMENTAL SECTION

Syntheses and Film Deposition. $Ga^{III}(L^{N2O3})]$ (**1**) and $[Zn^{II}(L^{N2O2})H_2O]$ (**2**) complexes were synthesized according to published procedures.[30,31] LB films were deposited on iron substrates using a KSV 2000 minitrough. The Langmuir−Blodgett (LB) films were deposited at the air|water interface at a surface pressure of 40 and 33 mN/m for **1** and **2**, respectively, with an average transfer ratio kept near unity.

Electron Passivation Studies. Electron passivation studies were performed using a three-electrode setup. Gold substrates coated with 13 LB layers of **1** or 11 LB layers of **2** were used as the working electrodes. Pt wire was used as the auxiliary electrode, and Ag/AgCl was used as the reference electrode.

Qualitative Corrosion Analysis. Corrosion experiments were performed using 99.5% iron foil substrates with 0.20 mm thickness. The substrates were abraded using 600 grade emery papers, polished with 0.05 micrometer alumina powder, then rinsed with ethanol and ultrapure water, and air dried. For agar gel experiments, the agar sample was prepared by using 0.25 g of agar, 2% phenolphthalein, 0.1 M $K_3[Fe^{III}(CN)_6]$, and 3% NaCl or 0.01 M H_2SO_4 depending on the acidic or saline corrosion. Scanning electron micrograph images were taken using a JSM-7600 FE scanning electron microscope.

Potentiodynamic Polarization Studies. Potentiodynamic polarization measurements were conducted using a CHI 650E electrochemical workstation. A three-electrode setup consisted of an iron foil with a surface area of 0.5 cm^2 as the working electrode, Ag/AgCl/saturated KCl as the reference electrode, and a Pt wire as the auxiliary electrode. 3.5% NaCl (w/v) and 0.01 M H_2SO_4 solutions were prepared from ultrapure water. All experiments were conducted at 25 °C. Tafel curves were obtained by scanning the electrode potential between −0.25 and 0.25 V vs open circuit potential with a scan rate of 10 mV/s. All the measurements were carried out in triplicate and the corrosion current values recorded as average ± standard deviation.

Electrochemical Impedance Spectroscopy. Electrochemical impedance spectroscopy data were collected using a CHI 650E electrochemical workstation. The iron substrate was the working electrode, a fresh carbon sheet (AvCarb MGL190, FuelCellStore, USA) was used as the counter electrode, and an Ag/AgCl electrode was used as the reference electrode. The electrolyte solution was 3.5% NaCl (w/v) or 0.01 M H_2SO_4. The initial potential of the working electrode was set at the open circuit potential. The frequency range was from 100 kHz to 0.01 Hz with an excitation amplitude of 5 mV. Data were collected at 12 points per decade of frequency. The samples were immersed in the corrosion test solutions (3.5% NaCl or 0.01 M H_2SO_4) for 30 min to reach equilibrium before the measurements. ZView 2.1 software was used to fit the data to an equivalent circuit (Figure S6). Table S1 and Table S2 summarize the fitting results. R_s represents the solution resistance between the Fe substrate and the reference electrode. R_{ct} is the charge transfer resistance at the metal/solution interface. The capacitance of the electrical double layer (C_{dl}) of the working electrode was modeled as a constant phase element.

UV−Visible Spectroscopy. UV−visible spectra were recorded with standard quartz cells at room temperature in 1.0×10^{-4} or 1.0×10^{-5} M wet methanol (2−3% water) solutions of **1**, **2**, $FeCl_2{\cdot}xH_2O$, or $FeCl_3{\cdot}xH_2O$ under aerobic conditions. A Shimadzu 3600 UV−vis−NIR spectrophotometer operating in the range of 190−1600 nm was utilized. Values of ε are given in M^{-1} cm^{-1}.

ASSOCIATED CONTENT

Supporting Information

The Supporting Information is available free of charge at https://pubs.acs.org/doi/10.1021/acs.langmuir.0c01826.

Details for the agar staining experiment, potentiodynamic polarization, and impedance spectroscopy (PDF)

AUTHOR INFORMATION

Corresponding Authors

Long Luo − *Department of Chemistry, Wayne State University, Detroit, Michigan 48202, United States;* orcid.org/0000-0001-5771-6892; Email: long.luo@chem.wayne.edu

Cláudio N. Verani − *Department of Chemistry, Wayne State University, Detroit, Michigan 48202, United States;* orcid.org/0000-0001-6482-1738; Email: cnverani@chem.wayne.edu

Authors

A. D. K. Isuri Weeraratne − *Department of Chemistry, Wayne State University, Detroit, Michigan 48202, United States*

Chathuranga C. Hewa-Rahinduwage − *Department of Chemistry, Wayne State University, Detroit, Michigan 48202, United States*

Complete contact information is available at: https://pubs.acs.org/10.1021/acs.langmuir.0c01826

Notes

The authors declare no competing financial interest.

https://dx.doi.org/10.1021/acs.langmuir.0c01826
Langmuir 2020, 36, 14173−14180

■ ACKNOWLEDGMENTS

This work is funded by the National Science Foundation through Grants NSF-CHE-1500201 and NSF-CHE1904584 to C.N.V., including partial support to A.D.K.I.W. L.L. thanks the Wayne State University for start-up funds. A.D.K.I.W is a recipient of a Thomas C. Rumble Fellowship from the Graduate School at WSU. We are particularly thankful to reviewer no. 2, whose comments prompted us to improve the manuscript significantly.

■ ABBREVIATIONS

AFM, atomic force microscopy
BAM, Brewster angle microscopy
E_{corr}, corrosion potential
H_2L^{N2O2}, 6,6′-(1*E*,1′*E*)-(4,5-bis(2-methoxyethoxy)-1,2-phenylene)bis(azan-1-yl-1-ylidene)bis(methan-1-yl-1-ylidene)bis(2,4-di-*tert*-butylphenol)
H_3L^{N2O3}, (6,6′-(2-(3,5-di-*tert*-butyl-2-hydroxybenzylamino)-4,5-bis(2-methoxyethoxy)phenylazanediyl)bis(methylene)-bis(2,4-di-*tert*-butylphenol)
i_{corr}, corrosion current
IE, inhibition efficiency
IRRAS, infrared reflection absorption spectroscopy
LB, Langmuir−Blodgett
LUMO, lowest unoccupied molecular orbital
SEM, scanning electron microscope

■ REFERENCES

(1) Koch, G. Cost of corrosion. In *Trends in Oil and Gas Corrosion Research and Technologies*; Elsevier, 2017; pp 3−30.
(2) Cui, J.; Yang, Y.; Li, X.; Yuan, W.; Pei, Y. Toward a slow-release borate inhibitor to control mild steel corrosion in simulated recirculating water. *ACS Appl. Mater. Interfaces* **2018**, *10*, 4183−4197.
(3) Heakal, F. E.-T.; Elkholy, A. E. Gemini surfactants as corrosion inhibitors for carbon steel. *J. Mol. Liq.* **2017**, *230*, 395−407.
(4) Ibrahim, S. Corrosion Inhibitors in the Oilfield. Version 1. Isalama, 2011 May 17. Available from: https://isalama.wordpress.com/article/corrosion-inhibitors-in-the-oilfield-3uf3kbfllnswt-4/.
(5) Ahmad, E. A.; Chang, H.-Y.; Al-Kindi, M.; Joshi, G. R.; Cooper, K.; Lindsay, R.; Harrison, N. M. Corrosion protection through naturally occurring films: New insights from iron carbonate. *ACS Appl. Mater. Interfaces* **2019**, *11*, 33435−33441.
(6) Snihirova, D.; Lamaka, S.; Taryba, M.; Salak, A.; Kallip, S.; Zheludkevich, M.; Ferreira, M.; Montemor, M. Hydroxyapatite microparticles as feedback-active reservoirs of corrosion inhibitors. *ACS Appl. Mater. Interfaces* **2010**, *2*, 3011−3022.
(7) Sastri, V. S. *Corrosion Inhibitors: Principles and Applications*; Wiley: New York, 1998.
(8) Li, L.; Swain, G. M. Effects of aging temperature and time on the corrosion protection provided by trivalent chromium process coatings on AA2024-T3. *ACS Appl. Mater. Interfaces* **2013**, *5*, 7923−7930.
(9) Vautrin-Ul, C.; Roux, F.; Boisse-Laporte, C.; Pastol, J. L.; Chausse, A. Hexamethyldisiloxane (HMDSO)-plasma-polymerised coatings as primer for iron corrosion protection: influence of RF bias. *J. Mater. Chem.* **2002**, *12*, 2318−2324.
(10) Carreira, A. F.; Pereira, A. M.; Vaz, E. P.; Cabral, A. M.; Ghidini, T.; Pigliaru, L.; Rohr, T. Alternative corrosion protection pretreatments for aluminum alloys. *J. Coat. Technol. Res.* **2017**, *14*, 879−892.
(11) Dina, A. N. Inhibition efficiency and corrosion rate studies of mild steel in nitric acid using 2-thioacetic acid-5-pyridyl-1, 3, 4-oxadiazole complexes. *Int. J. Corros. Scale Inhib.* **2019**, *8*, 717−725.
(12) Ibrahim, F.; Hammza, R.; Fadhil, D. Synthesis and characterization of Trimethoprim metal complexes used as corrosion inhibitors for carbon steel in acid media. *Int. J. Corros. Scale Inhib.* **2019**, *8*, 733−742.
(13) Moschona, A.; Plesu, N.; Mezei, G.; Thomas, A. G.; Demadis, K. D. Corrosion protection of carbon steel by tetraphosphonates of systematically different molecular size. *Corros. Sci.* **2018**, *145*, 135−150.
(14) Das, M.; Biswas, A.; Kundu, B. K.; Mobin, S. M.; Udayabhanu, G.; Mukhopadhyay, S. Targeted synthesis of cadmium (II) Schiff base complexes towards corrosion inhibition on mild steel. *RSC Adv.* **2017**, *7*, 48569−48585.
(15) Mishra, M.; Tiwari, K.; Mourya, P.; Singh, M.; Singh, V. P. Synthesis, characterization and corrosion inhibition property of nickel (II) and copper (II) complexes with some acylhydrazine Schiff bases. *Polyhedron* **2015**, *89*, 29−38.
(16) Keleş, H.; Emir, D. M.; Keleş, M. A comparative study of the corrosion inhibition of low carbon steel in HCl solution by an imine compound and its cobalt complex. *Corros. Sci.* **2015**, *101*, 19−31.
(17) Demadis, K. D.; Mantzaridis, C.; Raptis, R. G.; Mezei, G. Metal- Organotetraphosphonate Inorganic- Organic Hybrids: Crystal Structure and Anticorrosion Effects of Zinc Hexamethylenediamine-tetrakis (methylenephosphonate) on Carbon Steels. *Inorg. Chem.* **2005**, *44*, 4469−4471.
(18) Frey, M.; Harris, S. G.; Holmes, J. M.; Nation, D. A.; Parsons, S.; Tasker, P. A.; Winpenny, R. E. Elucidating the mode of action of a corrosion inhibitor for iron. *Chem. - Eur. J.* **2000**, *6*, 1407−1415.
(19) Thorpe, J. M.; Beddoes, R. L.; Collison, D.; Garner, C. D.; Helliwell, M.; Holmes, J. M.; Tasker, P. A. Surface Coordination Chemistry: Corrosion Inhibition by Tetranuclear Cluster Formation of Iron with Salicylaldoxime. *Angew. Chem., Int. Ed.* **1999**, *38*, 1119−1121.
(20) Mahdavian, M.; Tehrani-Bagha, A. R.; Alibakhshi, E.; Ashhari, S.; Palimi, M. J.; Farashi, S.; Javadian, S.; Ektefa, F. Corrosion of mild steel in hydrochloric acid solution in the presence of two cationic gemini surfactants with and without hydroxyl substituted spacers. *Corros. Sci.* **2018**, *137*, 62−75.
(21) Aslam, R.; Mobin, M.; Zehra, S.; Obot, I. B.; Ebenso, E. E. N, N'-Dialkylcystine Gemini and Monomeric N-Alkyl Cysteine Surfactants as Corrosion inhibitors on mild steel corrosion in 1 M HCl solution: A Comparative study. *ACS omega* **2017**, *2*, 5691−5707.
(22) El-Lateef, H. M. A.; Abo-Riya, M. A.; Tantawy, A. H. Empirical and quantum chemical studies on the corrosion inhibition performance of some novel synthesized cationic gemini surfactants on carbon steel pipelines in acid pickling processes. *Corros. Sci.* **2016**, *108*, 94−110.
(23) Zhu, Y.; Free, M. L.; Yi, G. The effects of surfactant concentration, adsorption, aggregation, and solution conditions on steel corrosion inhibition and associated modeling in aqueous media. *Corros. Sci.* **2016**, *102*, 233−250.
(24) Zhu, Y.; Free, M. L.; Yi, G. Electrochemical measurement, modeling, and prediction of corrosion inhibition efficiency of ternary mixtures of homologous surfactants in salt solution. *Corros. Sci.* **2015**, *98*, 417−429.
(25) Shubha, H.; Venkatesha, T.; Vathsala, K.; Pavitra, M.; Punith Kumar, M. Preparation of self assembled sodium oleate monolayer on mild steel and its corrosion inhibition behavior in saline water. *ACS Appl. Mater. Interfaces* **2013**, *5*, 10738−10744.
(26) Migahed, M.; Hegazy, M.; Al-Sabagh, A. Synergistic inhibition effect between Cu2+ and cationic gemini surfactant on the corrosion of downhole tubing steel during secondary oil recovery of old wells. *Corros. Sci.* **2012**, *61*, 10−18.
(27) Tehrani-Bagha, A. R.; Holmberg, K. Cationic ester-containing gemini surfactants: adsorption at tailor-made surfaces monitored by SPR and QCM. *Langmuir* **2008**, *24*, 6140−6145.
(28) El Achouri, M.; Infante, M. R.; Izquierdo, F.; Kertit, S.; Gouttaya, H.; Nciri, B. Synthesis of some cationic gemini surfactants and their inhibitive effect on iron corrosion in hydrochloric acid medium. *Corros. Sci.* **2001**, *43*, 19−35.
(29) Elachouri, M.; Hajji, M.; Salem, M.; Kertit, S.; Aride, J.; Coudert, R.; Essassi, E. Some nonionic surfactants as inhibitors of the corrosion of iron in acid chloride solutions. *Corrosion* **1996**, *52*, 103−108.

https://dx.doi.org/10.1021/acs.langmuir.0c01826
Langmuir 2020, 36, 14173−14180

(30) Gonawala, S.; Leopoldino, V. R.; Kpogo, K.; Verani, C. N. Langmuir-Blodgett films of salophen-based metallosurfactants as surface pretreatment coatings for corrosion mitigation. *Chem. Commun.* **2016**, *52*, 11155−11158.
(31) Weeraratne, A. I.; Hewa-Rahinduwage, C. C.; Gonawala, S.; Luo, L.; Verani, C. N. A Molecular Approach for Mitigation of Aluminum Pitting based on Films of Zinc (II) and Gallium (III) Metallosurfactants. *Chem. - Eur. J.* **2019**, *25*, 14048−14053.
(32) Zou, Y.; Wang, J.; Zheng, Y. Electrochemical techniques for determining corrosion rate of rusted steel in seawater. *Corros. Sci.* **2011**, *53*, 208−216.
(33) Wickramasinghe, L. D.; Mazumder, S.; Gonawala, S.; Perera, M. M.; Baydoun, H.; Thapa, B.; Li, L.; Xie, L.; Mao, G.; Zhou, Z.; Schlegel, H. B.; Verani, C. N. The Mechanisms of Rectification in Aul MoleculelAu Devices Based on Langmuir-Blodgett Monolayers of Iron(III) and Copper(II) Surfactants. *Angew. Chem., Int. Ed.* **2014**, *53*, 14462−14467.
(34) Wickramasinghe, L. D.; Perera, M. M.; Li, L.; Mao, G.; Zhou, Z.; Verani, C. N. Rectification in Nanoscale Devices Based on an Asymmetric Five-Coordinate Iron(III) Phenolate Complex. *Angew. Chem., Int. Ed.* **2013**, *52*, 13346−13350.
(35) The addition of the name Pockels to the films commonly known as Langmuir monolayers aims to rectify a historical omission toward the pioneering work of Agnes Pockels (1862−1935) in the understanding of film formation at the air/water surface. See the following references: Rayleigh, L.; Pockels, A. Surface tension. *Nature* **1891**, *43*, 437−439. (b) Pockels, A. On the relative contamination of the water-surface by equal quantities of different substances. *Nature* **1892**, *46*, 418−419. (c) Pockels, A. Relations between the surface-tension and relative contamination of water surfaces. *Nature* **1893**, *48*, 152−154. (d) Pockels, A. On the spreading of oil upon water. *Nature* **1894**, *50*, 223−224.
(36) Weeraratne, A. D. K. I.; Baydoun, H.; Shakya, R.; Niklas, J.; Xie, L.; Mao, G.; Stoian, S. A.; Poluektov, O. G.; Verani, C. N. Observation of current rectification by the new bimetallic iron(III) hydrophobe $[Fe^{III}_2(L^{N4O6})]$ on AulLB-moleculelAu devices. *Dalton Trans.* **2018**, *47* (40), 14352−14361.
(37) Shakya, R.; Hindo, S. S.; Wu, L.; Allard, M. M.; Heeg, M. J.; Hratchian, H. P.; McGarvey, B. R.; da Rocha, S. R. P.; Verani, C. N. Archetypical Modeling and Amphiphilic Behavior of Cobalt(II)-Containing Soft-Materials with Asymmetric Tridentate Ligands. *Inorg. Chem.* **2007**, *46*, 9808−9818.
(38) Kundu, S.; Datta, A.; Hazra, S. Effect of metal ions on monolayer collapses. *Langmuir* **2005**, *21*, 5894−5900.
(39) Ries, H. E., Jr Stable ridges in a collapsing monolayer. *Nature* **1979**, *281*, 287.
(40) Brand, I.; Juhaniewicz-Debinska, J.; Wickramasinghe, L.; Verani, C. N. An in situ spectroelectrochemical study on the orientation changes of an $[Fe^{III}L^{N2O3}]$ metallosurfactant deposited as LB Films on gold electrode surfaces. *Dalton Trans.* **2018**, *47*, 14218−14226.
(41) Perez, N. *Electrochemistry and Corrosion Science*; Springer, 2004; Vol. *412*, pp 80−89.
(42) Solomon, M. M.; Umoren, S. A.; Obot, I. B.; Sorour, A. A.; Gerengi, H. Exploration of dextran for application as corrosion inhibitor for steel in strong acid environment: effect of molecular weight, modification, and temperature on efficiency. *ACS Appl. Mater. Interfaces* **2018**, *10*, 28112−28129.
(43) Migahed, M.; Nasser, A.; Elfeky, H.; El-Rabiei, M. The synthesis and characterization of benzotriazole-based cationic surfactants and the evaluation of their corrosion inhibition efficiency on copper in seawater. *RSC Adv.* **2019**, *9*, 27069−27082.
(44) Singer, F.; Schlesak, M.; Mebert, C.; Höhn, S.; Virtanen, S. Corrosion properties of polydopamine coatings formed in one-step immersion process on magnesium. *ACS Appl. Mater. Interfaces* **2015**, *7*, 26758−26766.
(45) Dandia, A.; Gupta, S.; Singh, P.; Quraishi, M. Ultrasound-assisted synthesis of pyrazolo [3, 4-b] pyridines as potential corrosion inhibitors for mild steel in 1.0 M HCl. *ACS Sustainable Chem. Eng.* **2013**, *1*, 1303−1310.
(46) Schikorr, G. Über den Mechanismus des atmosphärischen Rostens des Eisens. *Mater. Corros.* **1963**, *14*, 69−80.

https://dx.doi.org/10.1021/acs.langmuir.0c01826
Langmuir 2020, 36, 14173−14180